LiDAR and UAV Photogrammetry Techniques for Optimizing 3D Mapping Inspection Systems of Reinforced Concrete Structures

Fabiola Yépez-Rincón[1*], Andrea N. Escobedo Tamez[1], Milena Mesa Lavista, Jorge Chávez Gómez[1], Adrián L. Ferriño Fierro[1], Gerardo J. Fajardo San Miguel[1], Saeid Pirasteh[2]

[1]Universidad Autónoma de Nuevo León, Faculty of Civil Engineering, FIC-UANL, Ciudad Universitaria, San Nicolás de los Garza, Nuevo León, C. P. 66455, México - fabiola.yepezrn@uanl.edu.mx

[2]Southwest Jiaotong University, Faculty of Geosciences and Environmental Engineering,Chengdu 611756, China -

Keywords: Concrete structure, Geomatics, LIDAR, NDE, Remote sensing, UAV

Abstract

This study addresses the challenges of accessibility and laborious intensity in visual inspections of public metropolitan mobility infrastructure, such as elevated Metro systems. It explores an experimental 3D-Mapping Inspection and Classification Evaluation method (3D-MICE) utilizing UAV imagery and geometric mensuration from 3D point clouds. The method introduces two classification techniques: Condition Classification by Intensity (CCI) and Geometry Classification by RGB color (GCC), applied to orthomosaics. 3D-MICE enables semi-automatic detection, segmentation, and measurement of cracks and stains in reinforced concrete by selecting areas of interest based on intensity and geometric features. This approach offers a promising, efficient, and precise alternative to traditional inspection methods. 3D-MICE can detect, segment and measure, semi-automatically, cracks and stains of reinforced concrete structures by selecting areas of interest based on intensity and geometry.

1. Introduction

All structures require inspections at varying intervals depending on their type and usage. Recently, many urban structures have become obsolete due to factors such as increased load demands, heightened contamination, and more intense hurricanes. Some authors (Hao et al., 2023; Lee & Ellingwood, 2017) recognize the future challenges for civil engineering structures to be multihazard resistant, resilient, and smart in response to climate uncertainties. Preventive maintenance and regular inspections enable decision-makers to detect issues early, take timely corrective actions, and ensure the structure functions as designed. Inspections are among the most effective measures to reduce maintenance costs and prevent catastrophic failures (Chen et al 2020; Mandirola et al., 2022). For instance, in Australia, annual maintenance expenses for civil infrastructure range from 0.4% to 2% of the initial construction costs (Mahmoodian et al., 2022). Inspection activities have intensified recently, with researchers from Geomatics and Civil Engineering contributing diverse inspection methodologies (Dolati et al, 2022). Examples of these inspections cover urban (Wetherley et al., 2017; Salem aet al, 2020), hydraulic (Zhang & Gao,2020), and transport infrastructures [10, 11]. The integration of remote sensing and robotic survey technologies enhances the quality, speed, affordability, and accessibility of inspections, while prioritizing safety and cost-effectiveness (Wetherley et al., 2017).

Unmanned Aerial Vehicle (UAV) has become one of the preferred techniques for infrastructure inspection, for example since 2013 [0001] used the synergy of LiDAR + RGB for data acquisition and analysis based on ground and aerial sensors.

Besides, pathology in structures is defined as the science dedicated to studying the problems or diseases that arise in buildings after they have been constructed (Pan et al, 2019). These injuries can appear in any part of a structure and can originate from many causes, which must be identified to solve them (Chen et al, 2019). The most common pathologies in RC elements are cracking, flaking, delamination, outliers, wear or abrasion, collision damage, polishing, and overload (McGuire, et al. 2016. Moreover, concrete has the capacity to resist high compressive stresses. However, it does not perform well under tensile and shearing stresses (Zhang & Gao,2020). RC structures are subjected to stresses and strains which depend on bending, axial load, shear and torsion (Pan et al, 2019). Steel bars could mitigate these stresses on the RC structure in areas where tensile and shearing stresses are expected to develop under service actions.

	TLS (Terrestrial Laser Scanning)	ALS (Airbone Laser Scanning)
Advantages	• Produces elaborated and precise point clouds. • Provides better control over point clouds, reducing redundant data during proocessing. • Easier	• More automated, less manual handling. • Can scan from different heights, capturing more points in less time. • Covers larger areas than TLS. • Effective for scanning large or hard-to-reach places.
Disadvantages	• Requires manual setup and repositioning. • Limited mobility, risk of incomplete or obstructed scans. • Large point clouds take longer to acquire. • Hard to access remote or difficult areas.	• Needs pre-planned flight paths to avoid excess data. • Strongly affected by weather conditions. • Generates heavy point clouds, requiring more complex and time consuming processing.

Table 1. Advantages and disadvantages of Terrestrial Laser Scanners (based on Kaartinen et al., 2022).

This contribution has been peer-reviewed. The double-blind peer-review was conducted on the basis of the full paper.
https://doi.org/10.5194/isprs-annals-X-3-W3-2025-145-2026

Cracks are breaks however, could appear in RC at different lengths, thicknesses, and depths, and are manifested externally in different elements of the structure with linear development. Cracks in concrete are attributed to multiple causes and can affect the appearance of a building and could indicate potential structural failure. Cracks can also indicate other problems, including poor concrete curing, shrinkage, thermal variations, chemical attack, external loads, excessive loads, errors in execution, errors in design, and differential displacement in foundations, among others (Gopalakrishnan et. al.2018; Dawood et al., 2018)

Researchers have studied structure strength and serviceability, including three principal basics: resistance, stiffness, and stability (Hao et al., 2023). Resistance refers to the ability of the structure to withstand the design loads. Stiffness means that there should be no deformations or vibrations that make users feel uncomfortable. Stability refers to the ability of the structure and all its elements to hold together and keep their original position over the years. Moreover, infrastructure durability is the ability to resist the action of weathering, chemical attack, abrasion, or any other deterioration process, and the durable concrete must maintain its original shape, quality, and service characteristics when exposed to this environment (ACI, 2016)

Besides, technologies based on sensor systems for inspecting structures have been evaluated (Wang, et al. 2020; Delatte et al., 2003). Visual inspection of big civil structures is generally used to detect surface defects such as cracks, spalling, and corrosion, among other deteriorations that produce an obvious change. Visual inspection is a subjective, labor intensive and costly method that can cause safety risks to the operators (Kim et al., 2015; Liang et al., 2020). Other Non-Destructive-Technique (NDT) methods that include remote sensors are capable of generating information such as images or point clouds that capture these defects (Adhikari et al., 2014). Several NDT methods use image detection to detect them (Kim et al., 2019) automatically. Challenges for the NDT methods are light conditions and the need for extra information for the analyses (Adhikari et al., 2014; Hutchinson et al., 2006).

Alternatively, Light detection and ranging (LiDAR) applied in terrestrial equipment such as Ground Laser Scanners (GLS), are used to produce 3D point clouds which are highly accurate and permit detection of the depth of the defects by capturing the XYZ dimensions (Mizoguchi et al., 2013). GLS emits laser pulses at high rates and registers the beam echoes on the receiver, obtaining, in addition to the spatial information, other values, such as the reflectivity of the object or intensity, that are collected for every point, and it's a function of the near-infrared spectral band (Liu et al., 2011), and the number of returns per pulse. GLS provides the required accuracy to calculate major and minor defects such as cracks (Olsen et al., 2013). Some authors consider photogrammetric techniques to be very efficient at detecting the texture of damaged surfaces (Lang et al.,2009; Guldur & Hajjar, 2016). Combining GLS with lower-cost technologies such as photogrammetry provides an opportunity for a synergistic method that can be more efficient in defect (Ghasemi et al., 2021; Demir & Baltsavias, 2012; Popescu et al., 2019). Different NDT studies applying LIDAR, photogrammetric technologies or their combinations are explained with research [30-33].

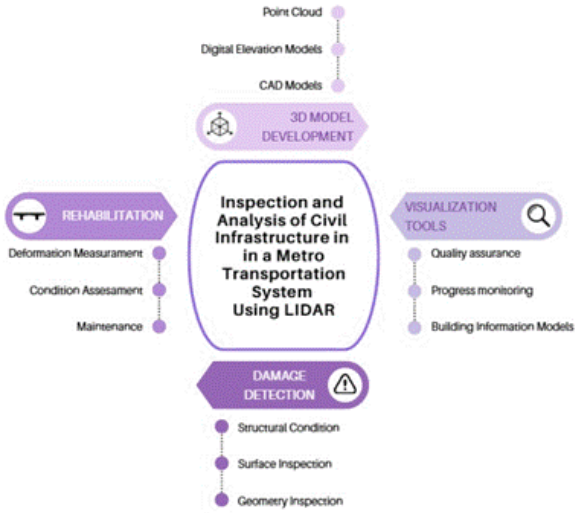

Figure 1. Applications of LIDAR for SHM (modified from Author, year).

The authors of this paper aim to determine the strengthen of the concrete structure and cracks. Nevertheless, this is a novel approach experimenting with a synergistic remote sensors tool called 3D-MICE for mapping, inspecting, classifying and evaluating the superficial deteriorations of reinforced concrete (RC) structures, using the synergy of LIDAR and photogrammetric technologies with aerial, mobile and ground platforms. This method uses the Condition classification by intensity (CCI), based on probability functions of the intensity and geometry, and the Geometry Classification by RGB images (TCC) that classifies 2D and orthomosaic true color images. 3D-MICE can semi-automatically detect, segment and measure cracks and stains on the concrete surfaces of the general structure. The method may improve future assessments to better understand the structures' condition and design future management, conservation, and mitigation practices.

This research recognizes the following critical points related to structural health monitoring of civil structures inspections:

- Need for systematic inspections: Preventive maintenance and regular inspections are essential to detect early deterioration, reduce costs, and avoid catastrophic failures.

- Understanding reinforced concrete pathologies: Common defects such as cracks, spalling, delamination, and corrosion must be identified, since they directly affect resistance, stiffness, stability, and durability.

- Advances in inspection technologies: Remote sensing and non-destructive techniques (e.g., UAVs, LiDAR, photogrammetry, and ground laser scanning) provide accurate,

safe, and cost-effective alternatives to traditional visual inspections.

- Innovation through integrated approaches: The proposed 3D-MICE method, combining LiDAR and photogrammetry, enables semi-automatic mapping, classification, and evaluation of surface deteriorations, offering a novel framework for improving structural health monitoring and future maintenance strategies.

2. Methodology

2.1 UAV-based LiDAR data acquisition

For this research, the Metro transportation system (Metro) located in Monterrey Metropolitan Area (MMA), North East Mexico, was used as a base element of civil engineering, representing an RC structure. This structure has cracks that have been enlarged since its construction in 1994. The Metro system comprises three Lines with a total length of 40.08 km. For this study, 1.09 km of Line 2 was examined, which has a total length of 13.75 km. This segment represents 2.73% of the total system and 7.96% of Line 2 length. This line has 2 defined parts, one elevated and the other underground. The elevated part is 6.76 km long with 214 columns. 67 of these columns were scanned based on visual inspection results, and 5 were selected to be analyzed (Figure 2).

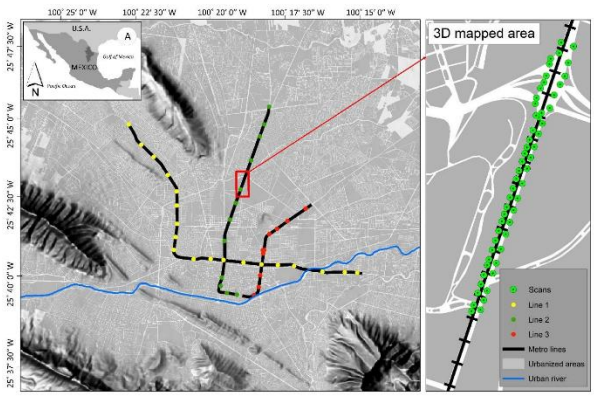

Figure 2. Location of the study area.

LiDAR sensor operated at a peak acquisition rate of 240,000 points per second and supported up to five returns per pulse, enabling detailed vertical structure characterization, particularly in densely vegetated areas. The resulting point clouds were processed, classified, and filtered to produce both a Digital Surface Model (DSM) and a bare-earth Digital Terrain Model (DTM), derived entirely from LiDAR data, with a spatial resolution of 5 cm. These high-resolution topographic datasets allowed for the accurate delineation of terrain features, identification of vegetated and built-up zones, and flood-prone area assessment (Zhang et al., 2019; Wang et al., 2021).

Figure 2 illustrates the complete methodological workflow implemented in this study, starting from UAV-based data acquisition and continuing through point cloud processing, building footprint digitization, topographic profile extraction, and flood risk analysis. This schematic provides a comprehensive overview of the sequential steps and the tools used at each stage, enabling replication and understanding of the integrated geospatial approach adopted for dam impact assessment.

2.1. Ground Laser Scanner (GLS)

A GLS-1500 unit by Topcon Co. achieves 4 mm accuracies at a 150 m range and 6” of angle (H&V) reference. The device has a class 1 laser, invisible and eye safe, using a 1,535 nm wavelength (not operational on water or other wet materials). Spot diameter of the laser is approximately 16 mm at a distance of 100 m. For this study, the distance was set to 80 m. Measurement speed reaches 30,000 points per second and captures intensity values and RGB data (2 megapixels) (Table 2).

Table 2. Technical specifications for the GLS-1500.

Parameters	Characteristics
Maximum range	90% reflectivity 330m
Maximum range	18% reflectivity 150m
Scanning mechanism	Rotating/oscillating
Single point accuracy (short range 1 to 70m and medium range 71- 150m)	2mm and 4mm respectively
Scan rate	30,000 points/second
Laser type	Pulsed (time of flight)
Wavelength	1535nm (invisible, eye-safe)
Captured data	Intensity values and RGB
Laser class	1

GLS emits laser pulses at high rates and registers the beam echoes on the receiver, obtaining, in addition to, spatial information. Other values, such as the object's reflectivity or intensity are collected for every point and are a function of the near-infrared spectral band (Brodu, N., & Lague, D. 2012) (Table 1), and the number of returns per pulse.

2.2. Unmanned Aerial Vehicle (UAV)

A low-cost multirotor DJI Phantom 4 Professional was used (Table 3). It has a maximum flight height range of 6000 m.a.s.l., with GPS / GLONASS positioning mode and an estimated flight time of 23 min (per battery/approximately), equipped with a 20 megapixels / FOV 94° camera (Dawood et al., 2018).

2.3 Digital cameras

A Nikon D5600 camera with a resolution of 24.2 megapixels and a sensor size of 23.5 mm x 15.6 mm was used for short-range photography. A GoPro Hero 6 camera with 12

This contribution has been peer-reviewed. The double-blind peer-review was conducted on the basis of the full paper.
https://doi.org/10.5194/isprs-annals-X-3-W3-2025-145-2026 | © Author(s) 2026. CC BY 4.0 License.

megapixels and 4K video mounted on a mobile platform with a stabilizer was used for mobile photography.

Table 3. Technical specifications for the UAV and camera sensor.

Parameters	Characteristics
Maximum height	6000 m.a.s.l.
Scanning mechanism	Rotating/oscillating
Sensor	1" CMOS Effective pixels: 20M
Lens	FOV 84° 8.8 mm/24 mm (35 mm format equivalent) f/2.8 – f/11 auto focus at 1 m – ∞
ISO Range	Video: 100 - 3200 (Auto) 100 - 6400 (Manual) Photo: 100 - 3200 (Auto) 100- 12800 (Manual)
Mechanical Shutter Speed	8 - 1/2000 s
Electronic Shutter Speed	8 - 1/8000 s

2.4. Previous visual inspection

A mobile survey was conducted in two series on each side of the elevated Metro Line. Complete coverage of the study section was obtained by placing the cameras facing north (front) and south (rear). It was necessary to conduct four photographic series, two series from each side of the avenue bordering the structure, so both sides of the structure were covered. In order to perform the four photographic series, the GoPro camera was mounted on the roof of a pickup truck using a suction cup adapter, and a time-lapse mode was set every 0.5 s.

2.5. Point cloud specifications and preparation

The complete 3D point cloud of the structure was produced by the synergy of the LiDAR and photogrammetry techniques explained below.

2.5.1. Point clouds produced with LIDAR (pcL)

A Leica FlexLine plus TS02 Topographic Total Station was used for geo-positioning control points on both sides of the Metro structure. At these points, the XYZ coordinates were obtained and marked on the sidewalks to position the scanner at known points and to reference the scans. The scans were performed by placing the scanner on the sidewalks at a distance between 15 and 20 m from the Metro structure. The GLS was placed at the height of approximately 1.5 m and a range distance of 80 m. Scans were performed at approximately 50 m intervals. The resolution for all scans was set to 0.002 m.

2.5.2. Point clouds produced with photogrammetry (pcP)

Two techniques were used to take the photographs of the Metro structure: (1) for short-range photogrammetry, a Nikon D5600 DSLR camera was used. The camera was placed at the height of 1.5 m and a distance of 15 - 20 m from the structure, with 70% overlap for post-processing photo alignments. (2) for aerial photogrammetry, a low-cost UAV was used, DJI Phantom IV pro, at the height of 40m and with a speed of 13 km / h. These settings were used in the upper section of the structure, with 75% overlap and around the selected columns.

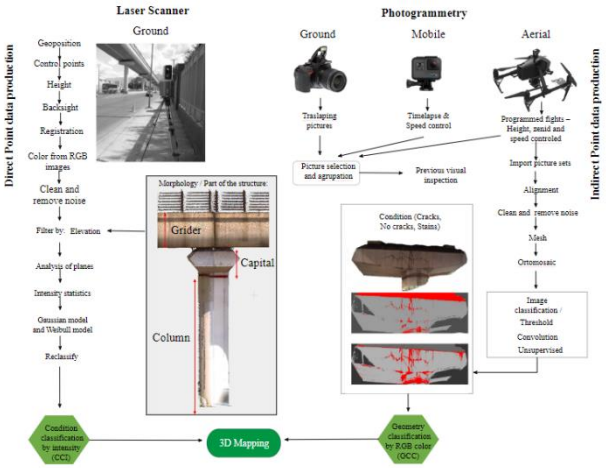

Figure 3. Workflow for 3D mapping, indicating point cloud data production GLS and photogrammetry, postprocessing and classifications by condition and geometrical analysis.

2.5.3. LiDAR Point Cloud treatment

All scans needed to be aligned to cover its entire surface and 3D form to fully visualize a column. To align and georeference the point clouds, the coordinates of the control points were used. When the scans are set in the registration process, points are aligned, and the noise has to be removed. Point clouds are visualized in intensity range (Figure 4A), but can also be observed in true color, using the RGB photos taken by the scanner (Figure 4B). The total point cloud was sectioned, and 5 columns were selected and exported into independent point clouds to facilitate its management use the.LAS format (Figure 4C).

The columns were selected using the previous visual inspection (UAV and GOPRO images). For each column, the most visible surface cracks were located and then exported using four steps: (1) the intensity ramp colors for the pcL, (2) the pcP in true color coloration and (3) corroborating its location with the observations made from the Google Earth, Street View program (from previous years) and the full set of photographs taken during this study with both the mobile and ground surveys.

Figure 4. A first view of the aligned structure. (A) The aligned point cloud displayed with intensities and (B) The aligned pcL merged with the RGB

2.6. 3D-MICE

2.6.1. Condition classification by intensity (CCI)

2.6.1.1. Filtering process

Four filters were used to segment the point clouds: (1) Intensity filter, which reclassifies the pcL according to the intensity range for each specific class, then implements the probability density functions. (2) Elevation filter reclassifies the selected pcL or pcP based on their absolute elevation value (Z). This filter was used to determine the elements of the structure (girder, capital and columns). (3) Analysis of planes filter, which finds and reclassifies groups of point clouds that form plane surfaces. It can specify different angles of flat surfaces (girder or capital faces) and does not require a reference surface to separate features, and (4) reclassify filters which reclassify all pcL that are at a specific elevation above or below a surface.

2.6.1.1. Intensity statistics and probability density functions

Similar areas of the structure were defined and grouped based on the statistical characteristics of intensity value for the pcL samples. A dense point cloud with intensity values from the GLS aloud to map the complete columns and shows an intensity profile that automatically detects the cracks and stains. By taking 7 to 11 samples from each part of the structure (girder, capital and column), their unique intensity ranges and frequency distribution can be determined.

Probability density functions have been used systematically in remote sensing research to understand the radiative transfer behavior of objects (Wang, W. et.al., 2018). Intensity ranges of the point clouds for each column and parts of the column were analyzed using two probability density functions: Gaussian and Weibull (Equations 1 and 2). (Mastin et al., 2009; Peppa et al., 2019; Kang & Doh, 2020).

Gaussian distribution

Eq. (1)

$$f(x)= \sqrt{((\lambda)/ \llbracket 2\pi x \rrbracket \hat{}(3)} \exp \llbracket (-(\lambda(x-\mu)\hat{}2)/(2\mu\hat{}2\ x) \rrbracket))$$

Where λλ is a continuous parameter (and is a continuous parameter)

Weibull distribution

Eq. (2)

$$f(x)= \alpha/\beta\ (x/\beta)\hat{}(\alpha-1)\exp\ (-(x/\beta)\hat{}\alpha\ )$$

Where αα is the continuous shape parameter (), and is the continuous parameter).

2.6.1.2. Morphology

The filter CANUPO (Girardeau-Montaut, 2016) was used to identify the morphological features that characterize pcL. This software distinguishes the heterogeneity of natural surfaces and their distinctive properties, allowing the automatic segmentation of pc. This allows the option to split angles and classes from the structural analysis (Barsanti et al, 2017; Corso et al, 2017; Sanchez Aparicio et al, 2019) using the CANUPO Class and CANUPO Confidence filters (Figure 7).

2.6.2. TCC

2.6.2.1. Supervised classification

Supervised classification of images and orthomosaics was performed. The algorithm used was the ISODATA clustering technique, for image recognition classification (Tou and Gonzales, 1974; Zaczek-Pepliska and Osinska-Skotak, 2018) and to automatically categorize the continuous raster data into discrete thematic groups with similar spectral-radiometric values. The clustering technique evaluates the similarities or differences of the pixel values then groups the pixels into separate classes. Several iterations of this process are required to reach a convergence threshold. The information obtained is used to map deteriorations in different classes (Figure 7).

2.6.2.2. Convolution and threshold filters

Gaussian convolution filters have been reported as an NDT for concrete (Fujita et al, 2008) or for bridge pavement (Sarmiento et al, 2019). Convolution filters were used as a common spatial enhancement operation that applies a matrix of small neighborhoods of cells (3x3 pixels) to compute a neighborhood average as the matrix moves with a non-directional edge filter to highlight the boundaries, or edges occurring between homogeneous groups, similar to Fujita et al, (2008). A supervised classification method using a threshold filter can be set as the numeric input, using chi-square statistics or Euclidean spectral distance. This process helps to delimit crack contours (Ozen & Guler, 2014).

3. Results

3.1. Visual inspection

The total studied area was represented by 67 columns of Metro Line 2. The visual inspection using Google Earth from past years, and the updated information from the surveys with UAV and the mobile photogrammetry (GoPro Hero 6), revealed that 95% of the capitals, 94% of the columns and 61% of the girder sections presented at least a small visually detectable crack. In the case of stains, they were found in 30% of the columns, 36% of the capitals and 18% of the girders (Figure 5).

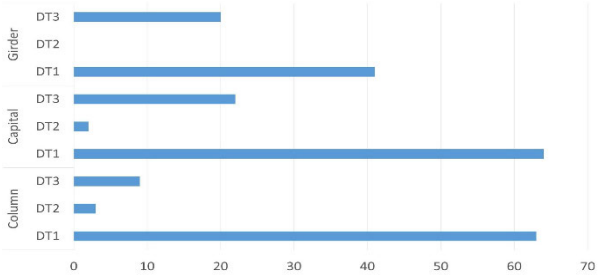

Figure 5. Concentration of the visual inspection of the 66 columns identifying three different deteriorations. Where H is the height of the column, DT1 are cracks, DT2 stains by stands and DT3 stains by others.

3.2. Intensity statistics and probability functions

The intensity values obtained with the GLS scans for each point cloud of the different deterioration types were from samples shown in Figure 6. Table 4 depicts the results of the probability density functions to estimate the intensity ranges in the different elements of the column for two types of damages. The samples obtained for cracking have a range of intensities ranging from 59 to 1024.17, and those from stained surfaces have a range for the samples obtained from 36 to 1529.41.

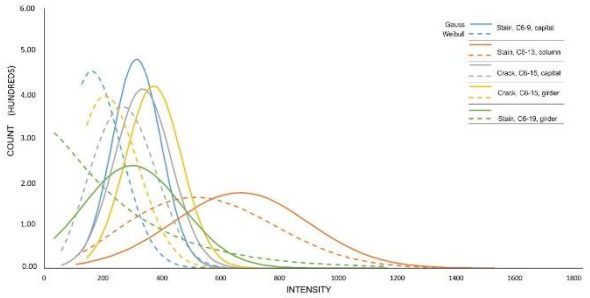

Figure 6. Distribution of relative frequencies of intensities in grouped classes for each element of the column and for the two different types of probability functions Gauss and Weibull. The distribution curves were plotted based on the intensity values obtained from the GLS scans.

3.2. Condition classification by intensity

3.2.1 Morphology

The application of the CANUPO software package in the different elements of the analyzed columns locates cracks in the concrete in a subtle way; the precision achieved by the GLS is such that it records this difference (Figure 7).

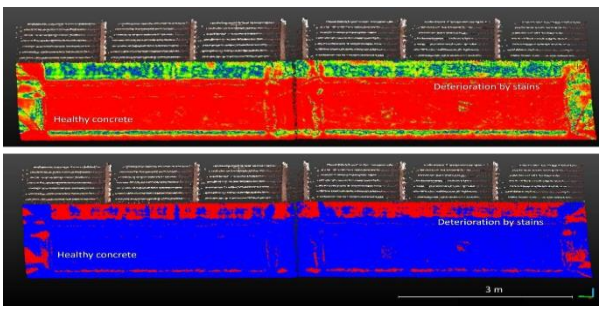

Figure 7. A girder section with two examples of cracks located with CANUPO above with filtering data by CANUPO Class and below by CANUPO Confidence filters.

3.3. Geometry classification

The heights of the columns along all line 2 varied from 4.42 m to 13.30 m. The girders were 1.9 m, and the capitals were 1.3 m. In the case of the studied section, the heights varied from 6.2 m to 8.8 m.

3.3.1 Threshold, convolution and unsupervised methods

The results obtained with the ISODATA algorithm indicate that classes of the concrete surface with different characteristics can be distinguished based on results using the 95% confidence interval. The combination of ISODATA, threshold and Gaussian convolution in the TCC allows an increment of precision of 15% compared to the CCI, which improves the 3D mapping of cracks.

3.4. 3D MICE

The overlay layer is the graphical representation of the 3D MICE indicating the location of every deterioration in each column and is displayed in Figure 8. Differences in stains caused by soot, a black substance formed during combustion, or separated from fuel during combustion, are evident on the sides of the Metro, especially in girders (Figure 8 D and F) and capitals (Figure 8 A-C and E).

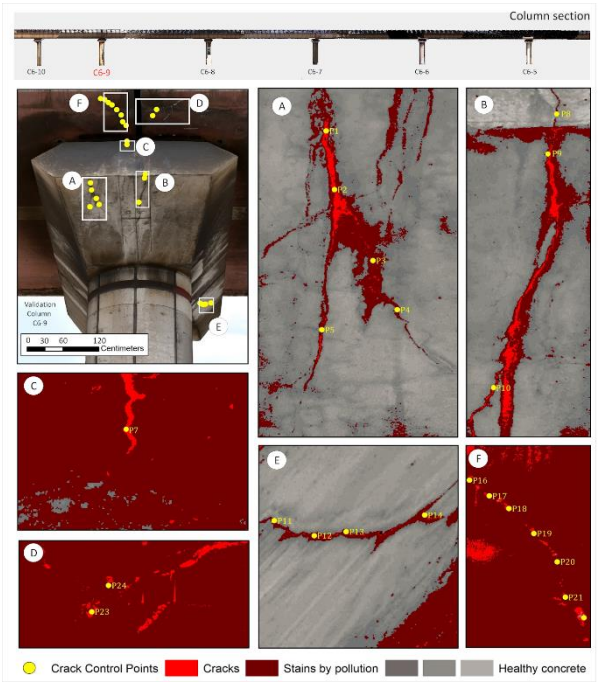

Figure 8. The graphical representation of mapping the deterioration using 3D MICE. Stains are dark red, cracks are bright red, and sound concrete is in different grays. Girders are represented by A, B, C and E, and Capital by D and F.

In addition, Table 4A and 4B illustrates the results from each selected column with several damages.

Table 4A. Statistics of sampled columns including the geometrical assessment where PE stands as Part of the element; D Description; NC Number of classes; MinI Minimum intensities; MaxI Minimum intensities.

Code	PE	D	NC	MinI	MaxI
C1-9	Capital	Stain	62	129	773.44

C1-13	Column	Stain	49	109	1529.41
C1-15	Capital	Crack	62	59	1024.18
C1-15	Girder	Crack	62	145	957.68
C1-19	Girder	Stain	62	36	1164.50

Table 4B. Statistics of sampled columns including the geometrical assessment where SD Standard deviation; S is the Total damaged area; CP Control points; MWC Matched with cracks.

Gauss distribution		Weibull distribution		S (m^2)	No. CP	CP MWC
Mean	**SD**	**alfa**	**beta**	8.34	24	18
314.47	82.99	2.30	208.54	7.24	18	17
667.35	229.37	2.54	626.27	5.26	23	15
335.05	96.53	2.91	307.71	8.25	24	18
372.12	95.05	2.51	255.06	4.62	25	17
300.09	168.84	1.06	267.99	8.34	24	18

4. Discussion

Through systematic surveys of the Metro system using the GLS and UAV processed with 3D MICE, the condition of this RC structure was able to be assessed. 3D MICE is based on CCI and TCC processes, by which it was possible to inspect a section of a transport system RC structure, scanning 67 columns and analyzing 7.69% of the whole transport system.

CCI analyzes pcL using CANUPO filters to determine sections and identify cracks and stains based on the morphology of the surface. This filter obtains an 85% effectiveness in identifying cracks and stains. However, this result varies depending on the element of the structure, being more effective on the capitals and girders than the columns. The filter didn´t work with the columns because of the decorative indentations that run along it, which creates repetitive changes in the form, so the filter overestimates as damage to the columns.

The morphology filter used in CANUPO is similar to other methods using the point cloud to visualize morphological details in reinforced concrete structures. Virtual Reality (Omer, M., et.al. 2019) and Point Net methods (Nasrollahi, M., et.al. 2019) use the information and transform it into images to carry out the inspection and locate the cracks. However, the method requires advanced hardware requirements for larger sections, but with 3D MICE, you can choose a specific section, based on a previous visual inspection and focus on it with a smaller set of points requiring lower hardware requirements.

A CANUPO limitation is it only displays two types of defects, that's why you have to run it twice, one for the cracks and another one for the stains. However, this limitation was solved with the use of the TCC method. Moreover, TCC uses the processes threshold, convolution and supervised classification of the images to locate the different classes like cracks, stains and sound concrete in one run compared with the two needed with CCI using CANUPO.

Furthermore, the TCC uses RGB images taken from aerial angles with the use of UAV and through a photogrammetric process pcP were obtained. This data covers blind spots on pcL information of the images obtained from ground level by the GLS. The TCC processing also uses trained sites to determine the classes of interest complementing the CCI information, increasing up to 15% in mapping deterioration in the reinforced concrete structure. The use of 3D MICE allows precise estimations of cracks, stains location and dimensions throughout time.

5.Conclusions

3D MICE method speeds up data collection and helps monitor the structure and identify changes that could affect its operation. It also eliminates the risk of carrying out measurements on RC structures with great height. 3D MICE can detect, segment and measure, semi-automatically, cracks and stains on reinforced concrete surfaces. It can also obtain geometric characteristics of the structure with a precision of 0.002m.

The advantages of 3D MICE over other similar methods are based on the complementary data produced with LIDAR and photogrammetry technologies, focusing on specific sections of the RC structure for a deeper analysis.

3D MICE can be of special interest to civil engineers and metropolitan administrative agencies as a base of information for the inspection advice system that can be used for structures of interest, historical buildings, and very crowded structures, among others.

Results can be of special interest to civil engineers and metropolitan administrative agencies as base information for the inspection advice system. This could result in less investment, time, and lower risk for the personnel involved in gathering information.

6. Acknowledgements

The authors express their gratitude to PROVERICYT supporting bachelor students, PAICYT and SEP-PRODEP for the financial support of research projects IT636-18 and 511-6/17/7538, respectively.

7. References

American Concrete Institute, Guide to Durable Concrete, 2016). Barsanti, S.G., Guidi, G. and De Luca, L., 2017. Segmentation of 3D models for cultural heritage structural analysis–some critical issues. ISPRS Annals of the Photogrammetry, Remote Sensing and Spatial Information Sciences, 4, p.115.

Chen, Changkun, Lili Xu, Dongyue Zhao, Tong Xu, and Peng Lei. (2020). A new model for describing the urban resilience considering adaptability, resistance and recovery; Safety science 128, DOI: https://doi.org/10.1016/j.ssci.2020.104756

Chen, S., Laefer, D. F., Mangina, E., Zolanvari, S. I., & Byrne, J.(2019). UAV bridge inspection through evaluated 3D reconstructions. Journal of Bridge Engineering, 24(4), 05019001. https://ascelibrary.org/doi/pdf/10.1061/%28ASCE%29BE. 1943-5592.0001343 8

Corso, J., Roca, J. and Buill, F., 2017. Geometric analysis on stone façades with terrestrial laser scanner technology. Geosciences, 7(4), p.103.

Dawood T., Zhu Z., Zayed T. (2018) Detection and Quantification of Spalling Distress in Subway Networks. In: Chau K., Chan I., Lu W., Webster C. (eds) Proceedings of the 21st International Symposium on Advancement of Construction Management and Real Estate. Springer, Singapore. DOI: https://doi.org/10.1007/978-981-10-6190-5_55

Delatte, N., Chen, S. E., Maini, N., Parker, N., Agrawal, A., Mylonakis, G., & Miller, R. (2003). Application of nondestructive evaluation to subway tunnel systems. Transportation Research Record: Journal of the Transportation Research Board, (1845), 127-135. DOI: https://doi.org/10.3141/1845-14

Demir, N., & Baltsavias, E. (2012). Automated modeling of 3D building roofs using image and LiDAR data. In Proceedings of the XXII Congress of the International Society for Photogrammetry, Remote Sensing, Melbourne, Australia (Vol. 25). DOI: https://doi.org/10.5194/isprsannals-I-4-35-2012

Dolati, S. S. K., Mehrabi, A., Dolati, S. S. K., & Caluk, N. (2022, April). NDT methods for damage detection in steel bridges. In Health Monitoring of Structural and Biological Systems XVI (Vol. 12048, pp. 385-394). SPIE.

Dawood, T., Zhu, Z., & Zayed, T. (2018). Computer vision–based model for moisture marks detection and recognition in subway networks. Journal of Computing in Civil Engineering, 32(2), 04017079. DOI: https://doi.org/10.1061/(ASCE)CP.1943-5487.0000728

Fujita, Y., Mitani, Y. & Hamamoto, Y., (2006). A method for crack detection on a concrete structure. In 18th International Conference on Pattern Recognition (ICPR'06) (Vol. 3, pp. 901-904). IEEE. DOI; https://doi.org/10.1109/ICPR.2006.98

Ghasemi M., Varshosaz M., Pirasteh S. , Shamsipour G. (2021).Optimizing Sector Ring Histogram of Oriented Gradients for human injured detection from drone images, Geomatics, Natural Hazards and Risk. 12:1, 581-604, DOI: 10.1080/19475705.2021.1884608.

Girardeau-Montaut, D., 2016. CloudCompare. Gopalakrishnan, K., Gholami, H., Vidyadharan, A., Choudhary, A., & amp; Agrawal, A. (2018). Crack damage detection in unmanned aerial vehicle images of civil infrastructure using pre-trained deep learning model. International Journal for Traffic and Transport Engineering, 8, 1. DOI: https://doi.org/10.7708/ijtte.2018.8(1).01

Guldur, B., & Hajjar, J. F. (2016). Automated classification of detected surface damage from point clouds with supervised learning. In ISARC. Proceedings of the International Symposium on Automation and Robotics in Construction (Vol. 33, p. 1). IAARC Publications. DOI: structure defect detection. Experimental Techniques, 35(6), 27-34. DOI: https://doi.org/10.1111/j.1747-1567.2010.00644.x

Hao, H., Bi, K., Chen, W., Pham, T. M., & Li, J. (2023). Towards next generation design of sustainable, durable, multi-hazard resistant, resilient, and smart civil engineering structures. Engineering Structures, 277, 115477.

Hutchinson, T.C. and Chen, Z. (2006). Improved image analysis for evaluating concrete damage. Journal of Computing in Civil Engineering, vol. 20, no. 3, pp. 210-216. DOI: https://doi.org/10.1061/(ASCE)0887-3801(2006)20:3(210)

Kang, J., & Doh, N. L. (2020). Automatic targetless camera–LIDAR calibration by aligning edge with Gaussian mixture model. Journal of Field Robotics, 37(1), 158-179. DOI: https://doi.org/10.1002/rob.21893

Kim, H., Ahn, E., Shin, M., & Sim, S. H. (2019). Crack and noncrack classification from concrete surface images using machine learning. Structural Health Monitoring, 18(3), 725-

738. DOI: https://doi.org/10.1177/1475921718768747 Kim, M. K., Sohn, H., & Chang, C. C. (2015). Localization and quantification of concrete spalling defects using terrestrial laser scanning. Journal of Computing in Civil Engineering, 29(6), 04014086. DOI: https://doi.org/10.1061/(ASCE)CP.1943-5487.0000415

Lang M. W. and G. W. McCarty. (2009). “Lidar intensity for improved detection of inundation below the forest canopy,” Wetlands, vol. 29, no. 4, pp. 1166–1178. DOI: https://doi.org/10.1672/08-197.1

Liu, W., Chen, S., & Hauser, E. (2011). LiDAR-based bridge structure defect detection. Experimental Techniques, 35(6), 27-34. DOI: https://doi.org/10.1111/j.1747-1567.2010.00644.x

Lee, J. Y., & Ellingwood, B. R. (2017). A decision model for intergenerational life-cycle risk assessment of civil infrastructure exposed to hurricanes under climate change. Reliability Engineering & System Safety, 159, 100-107.

Liang, Y., Xu, K., & Zhou, P. (2020). Mask Gradient Response-Based Threshold Segmentation for Surface Defect Detection of Milled Aluminum Ingot. Sensors, 20(16), 4519. DOI: https://doi.org/10.3390/s20164519

Mandirola, M., Casarotti, C., Peloso, S., Lanese, I., Brunesi, E.,& Senaldi, I. (2022). Use of UAS for damage inspection and assessment of bridge infrastructures. International Journal of Disaster Risk Reduction, 72, 102824

Mahmoodian, M., Shahrivar, F., Setunge, S., & Mazaheri, S. (2022). Development of digital twin for intelligent maintenance of civil infrastructure. Sustainability, 14(14), 8664.

Mizoguchi, T., Koda, Y., Iwaki, I., Wakabayashi, H., Kobayashi, Y., Shirai, K., & Lee, H. S. (2013). Quantitative scaling evaluation of concrete structures based on terrestrial laser scanning. Automation in construction, 35, 263-274. DOI: https://doi.org/10.1016/j.autcon.2013.

Nasrollahi, M., Bolourian, N., & Hammad, A. (2019, June). Concrete surface defect detection using deep neural network based on lidar scanning. In Proceedings of the CSCE Annual Conference, Laval, Greater Montreal, QC, Canada (pp. 12-15).

Olsen, M. J., Chen, Z., Hutchinson, T., & Kuester, F. (2013).Optical techniques for multiscale damage assessment. Geomatics, Natural Hazards and Risk, 4(1), 49-70. DOI: https://doi.org/10.1080/19475705.2012.670668

Omer, M., Margetts, L., Hadi Mosleh, M., Hewitt, S., & Parwaiz, M. (2019). Use of gaming technology to bring bridge inspection to the office. Structure and Infrastructure Engineering, 15(10), 1292-1307.

Ozen, M., & Guler, M. (2014). Assessment of optimum thresholdand particle shape parameter for the image analysis of aggregate size distribution of concrete sections. Optics and Lasers in Engineering, 53, 122-132. DOI: https://doi.org/10.1016/j.optlaseng.2013.

Pan, Y., Dong, Y., Wang, D., Chen, A.,& Ye, Z. (2019). Three-

dimensional reconstruction of structural surface model of heritage bridges using UAV-based photogrammetric point clouds. Remote Sensing, 11(10), 1204. DOI: https://doi.org/10.3390/rs11101204 9

Peppa, M. V., Hall, J., Goodyear, J., & Mills, J. P. (2019). Photogrammetric assessment and comparison of DJI Phantom 4 pro and phantom 4 RTK small unmanned aircraft systems. ISPRS Geospatial Week 2019. DOI: https://doi.org/10.5194/isprs-archives-XLII-2-W13-503-2019, 2019

Popescu, C., Täljsten, B., Blanksvärd, T., & Elfgren, L. (2019). 3D reconstruction of existing concrete bridges using optical methods. Structure and Infrastructure Engineering, 5(7), 912-924 DOI: https://doi.org/10.1080/15732479.2019.1594315

Salem, M., Tsurusaki, N., & Divigalpitiya, P. (2020). Landuse/ land cover change detection and urban sprawl in the peri-urban area of greater Cairo since the Egyptian revolution of 2011. Journal of Land Use Science, 1-15. DOI: https:// doi.org/10.1080/1747423

Sánchez-Aparicio, L.J., Del Pozo, S., Rodríguez-Gonzálvez, P., Muñoz-Nieto, Á.L., González-Aguilera, D. & Ramos, L.F. (2019). Integral diagnosis and structural analysis of historical constructions by terrestrial laser scanning. Laser Scanning: An Emerging Technology in Structural Engineering, 14, p.169. DOI: https://doi.org/10.1201/9781351018869-11

Sarmiento, J.S., Rosales, C.A.M. & Fajardo, A.C., 2019, April. Non-destructive Bridge Pavement Detection Using Impact Sound and Convolutional Neural Network. In Nguyen et. al. (2020). DOI: https://doi.org/10.1145/3330482.3330521

Tou J. T., Gonzales R. C. (1974): Pattern Recognition Principles. Reading, Massachusetts: Addison-Wesley Publishing Company, 1974.

Wang, L., Xu, S., Qiu, J., Wang, K., Ma, E., Li, C., & Guo, C. (2020). Automatic monitoring system in underground engineering construction: review and prospect. Advances in Civil Engineering, 2020. DOI: https://doi.org/10.1155/2020/3697253

Wang, L., Xu, S., Qiu, J., Wang, K., Ma, E., Li, C., & Guo, C. (2020).Automatic monitoring system in underground engineering construction: review and prospect. Advances in Civil Engineering, 2020. DOI: https://doi.org/10.1155/2020/3697253

Wang, W., Nemani, R., Hashimoto, H., Ganguly, S., Huang, D.,Knyazikhin, Y., ... & Bala, G. (2018). An interplay between photons, canopy structure, and recollision probability: A review of the spectral invariants theory of 3d canopy radiative transfer processes. Remote Sensing, 10(11), 1805.

Wetherley, E. B., Roberts, D. A., & McFadden, J. P. (2017). Mapping spectrally similar urban materials at sub-pixel scales. Remote Sensing of Environment, 195, 170-183 DOI: https://doi.org/10.1016/j.rse.2017.04.013

Zaczek-Peplinska, J. and Osińska-Skotak, K., 2018. Concrete surface evaluation based on the reflected TLS laser beam's intensity image classification. Studia Geotechnica et Mechanica, 40(1), pp.56-64.

Zhang, S., & Gao, H. (2020). Using the Digital Elevation Model (DEM) to improve the spatial coverage of the MODIS based reservoir monitoring network in South Asia. Remote Sensing, 12(5), 745. https://doi.org/10.3390/ rs12050745